INTEGRABLE CROSS-FIELD GENERATION BASED ON IMPOSED SINGULARITY CONFIGURATION – THE 2D MANIFOLD CASE –

Jovana Jezdimirović[1] Alexandre Chemin[2] Jean-François Remacle[2]

[1] *Siemens Digital Industries Software, Leuven, Belgium jovana.jezdimirovic@siemens.com*
[2] *Université catholique de Louvain, Louvain la Neuve, Belgium*
alexandre.chemin@uclouvain.be, jean-francois.remacle@uclouvain.be

ABSTRACT

This work presents the mathematical foundations for the generation of integrable cross-field on 2D manifolds based on user-imposed singularity configuration. In this paper, we either use singularities that appear naturally by solving a non-linear problem, or use as an input user-defined singularity pattern, possibly with high valence singularities that typically do not appear in cross-field computations. This singularity set is under the constraint of Abel-Jacobi's conditions for valid singularity configurations. The main contribution of the paper is the development of a formulation that allows computing, when possible, an integrable isotropic 2D cross-field from a given set of singularities through the resolution of only two linear PDEs. To address the issue of possible suboptimal singularities' distribution, we also present the mathematical setting for the generation of an integrable anisotropic 2D cross-field based on a user-imposed singularity pattern. The developed formulations support both an isotropic and an anisotropic block-structured quad mesh generation.

Keywords: integrable 2D cross-field, valid singularity configuration, quad mesh

1. INTRODUCTION AND RELATED WORK

The cross-field guided techniques represent a significant member of the quad meshing methods' family, accompanied by a noteworthy number of methods [1, 2, 3]. The cross-field drives the orientation and the size of quadrilaterals of a quad mesh, and there exists a profound topological relationship between them [4]. It is important to note that the *integrability* represents a crucial feature of a cross-field, used to obtain a conformal parameterization, *e.g.*, [5, 6], finite length of integral lines, and even influence the number of singularities, *e.g.*, [7]. Nevertheless, cross-fields are not integrable by default. Here, we mention the works closest to our approach and direct the reader to other prominent methods *e.g.*, [8, 9, 10, 11] for a more detailed overview.

Computing an integrable cross-field can be achieved by, for instance, using the Hodge decomposition [6, 12], reducing the curl [7], obtaining the metric which is flat except at singularities [13, 14, 15], using the trivial connection [16], or computing a global conformal scaling from curvature prescription [4, 5]. Some of the techniques also consider a flat metric with cone singularities but do not consider additional constraints needed for quadrangulation [17, 18], or obtain conformal parametrization on the prescribed singularity set, but do not take into account the holonomy signature which may result that obtained parameterization is not aligned with the given field [19]. The work of [6] generates an integrable vector field from a given frame field relying on the Hodge decomposition. At the same time, using the Hodge decomposition as in [12] is computationally intensive and may not preserve the directions, while reducing the curl in the post-

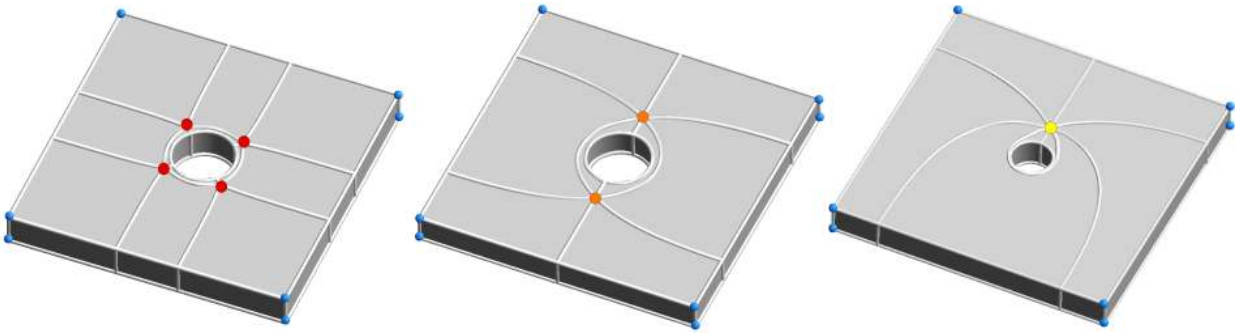

Figure 1: Three quad layouts of a simple domain. Singularities of valence 3 are colored in blue, valence 5 in red, valence 6 in orange, and valence 8 in yellow.

processing step as in [7] may not eliminate the curl entirely. A trivial connection [16], a flat metric with zero holonomy around non-contractible cycles, can indeed be used to obtain an integrable direction field with user-specified singularities, but the boundary alignment constraints may not be honored. We compute a metric resembling the one presented in the method relying on Abel-Jacobi theory [13, 14, 15], but without using the meromorphic quartic differentials. The techniques of [4, 5] present a close concept to the one developed in this paper in terms that the computed size field is obtained from the singularity set. The work of [5] involves using the iterative process to identify the locations and the curvatures of singularities and computing the target metric by solving the linear systems of the Poisson equations. Our approach uses an imposed singularity set, as an application-dependent matter, and exploits the commuting of vector fields under the Lie bracket to obtain the guiding size field by solving two linear systems.

Unlike the previously mentioned methods, we develop the integrability formulation for both isotropic and anisotropic scaling. Further, our formulation offers a simple manner of computing the relevant size field and effortless singularity set imposing. Last but not least, the generated cross-field induces per-partition bijective parametrization, more details in [20].

Although leaning on heterogeneous approaches, all quad-meshing methods share the common challenge: dealing with the inevitable singularity configuration. A *singularity* appears where a cross-field vanishes and it represents an irregular vertex of a quad layout/quad mesh [3], *i.e.*, a vertex which doesn't have exactly four adjacent quadrilaterals. The singular configuration is constrained by the Euler characteristic χ, which is a topological invariant of a surface. Moreover, a suboptimal number or location of singularities can have severe consequences: causing undesirable thin partitions, large distortion, not an adequate number and/or tangential crossings of separatrices as well as *limit cycles* (spiraling separatrices) [21, 22, 2].

Our integrable cross-field formulation, with mathematical foundations detailed in Section 2, exploits the concept of user-imposed singularity configuration in order to gain direct control over their number, location, and valence (number of adjacent quadrilaterals). The user is entitled to use either naturally appearing singularities, obtained by solving a non-linear problem [23, 2, 24, 25], using globally optimal direction fields [26], or to impose its own singularity configuration, possibly with high valences, as illustrated in Fig. 1. It is important to note that the choice of singularity pattern is not arbitrary, though. Moreover, it is under the direct constraint of *Abel-Jacobi theory* [13, 14, 15] for valid singularity configurations. Here, the singularity configuration is taken as an input and an integrable isotropic cross-field is computed by solving only two linear systems, Section 3. Finally, the preliminary results of the developed cross-field formulation for an isotropic block-structured quad mesh generation are outlined using the 3-step pipeline [20] in Section 4.

Computing only one scalar field H (a metric that is flat except at singularities) imposes a strict constraint on singularities' placement, *i.e.*, fulfilling all Abel-Jacobi conditions. In practice, imposing suboptimal distribution of singularities may lead to not obtaining a boundary-aligned cross-field, preventing an isotropic quad mesh generation, Section 4.1 and 4.2. To bypass this issue, we develop a new cross-field formulation on the imposed singularity configuration, which considers the integrability, while relaxing the condition on isotropic scaling of crosses' branches. Here, two independent metrics H_1 and H_2 are computed instead of only one as in the Abel-Jacobi framework, enabling an integrable 2D cross-field generation with anisotropic scaling without modifying singularity configuration imposed by the user, Section 5.

Lastly, final remarks and some of the potential appli-

cations are discussed in Section 6.

2. CROSS-FIELD COMPUTATION ON PRESCRIBED SINGULARITY CONFIGURATION

We define a 2D cross $\mathbf{c}$ as a set of 2 unit coplanar orthogonal vectors and their opposite, *i.e.*,

$$\mathbf{c} = \{\mathbf{u}, \mathbf{v}, -\mathbf{u}, -\mathbf{v}\}$$

with $\{\mathbf{u}.\mathbf{v} = 0,\ |\mathbf{u}| = |\mathbf{v}| = 1\}$ and $\mathbf{u}, \mathbf{v}$ are coplanar. These vectors are called cross' branches.

A 2D cross-field $\mathcal{C}_\mathcal{M}$ on a 2D manifold $\mathcal{M}$, now, is a map $\mathcal{C}_\mathcal{M} : \mathbf{X} \in \mathcal{M} \rightarrow \mathbf{c}(\mathbf{X})$, and the standard approach to compute a smooth boundary-aligned cross-field is to minimize the Dirichlet energy:

$$\min_{\mathcal{C}_\mathcal{M}} \int_\mathcal{M} \|\nabla \mathcal{C}_\mathcal{M}\|^2 \tag{1}$$

subject to the boundary condition $\mathbf{c}(\mathbf{X}) = \mathbf{g}(\mathbf{X})$ on $\partial\mathcal{M}$, where $\mathbf{g}$ is a given function.

The classical boundary condition for cross-field computation is that $\forall \mathbf{P} \in \partial\mathcal{M}$, with $\mathbf{T}(\mathbf{P})$ a unit tangent vector to $\mathcal{M}$ at $\mathbf{P}$, one branch of $\mathbf{c}(\mathbf{P})$ has to be colinear to $\mathbf{T}(\mathbf{P})$. In the general case, there exists no smooth cross-field matching this boundary condition. The cross-field will present a finite number of singularities $\mathbf{S}_j$, located at $\mathbf{X}_j$ and of index k_j, related to the concept of valence as $k_j = 4 - \text{valence}(\mathbf{S}_j)$.
We define a singularity configuration as the set

$$\mathcal{S} = \{\mathbf{S}_j, j \in [|1, N|], N \in \mathbb{Z}\}.$$

In the upcoming section, a method to compute a cross-field $\mathcal{C}_\mathcal{M}$ matching a given singularity configuration $\mathcal{S}$ is developed. In other words, we are looking for $\mathcal{C}_\mathcal{M}$ such as:

$$\begin{cases} \cdot \text{ if } \mathbf{X} \text{ belongs to } \partial\mathcal{M}, \text{ at least one branch of} \\ \quad \mathcal{C}_\mathcal{M}(\mathbf{X}) \text{ is tangent to } \partial\mathcal{M}, \\ \cdot \text{ singularities of } \mathcal{C}_\mathcal{M} \text{ are matching the given } \mathcal{S} \\ \quad \text{(the same number, location, and indices).} \end{cases} \tag{2}$$

Before developing the method to compute such a cross-field, a few operators on the 2D manifold have to be defined.

2.1 Curvature and Levi-Civita connection on the 2D manifold

Let E^3 be the Euclidean space equipped with a Cartesian coordinates system $\{x^i, i = 1, 2, 3\}$, and $\mathcal{M}$ be an oriented two-dimensional manifold embedded in E^3. We note $\mathbf{n}(\mathbf{X})$ the unit normal to $\mathcal{M}$ at $\mathbf{X} \in \mathcal{M}$. It is assumed that the normal field $\mathbf{n}$ is smooth and that the Gaussian curvature K is defined and smoothed on $\mathcal{M}$.

If $\gamma(s)$ is a curve on $\mathcal{M}$ *parametrized by arc length*, the Darboux frame is the orthonormal frame defined by

$$\mathbf{T}(s) = \gamma'(s) \tag{3}$$
$$\mathbf{n}(s) = \mathbf{n}(\gamma(s)) \tag{4}$$
$$\mathbf{t}(s) = \mathbf{n}(s) \times \mathbf{T}(s). \tag{5}$$

One then has the differential structure

$$\mathrm{d}\begin{pmatrix} \mathbf{T} \\ \mathbf{t} \\ \mathbf{n} \end{pmatrix} = \begin{pmatrix} 0 & \kappa_g & \kappa_n \\ -\kappa_g & 0 & \tau_r \\ -\kappa_n & -\tau_r & 0 \end{pmatrix} \begin{pmatrix} \mathbf{T} \\ \mathbf{t} \\ \mathbf{n} \end{pmatrix} \mathrm{d}s \tag{6}$$

where κ_g is the geodesic curvature of the curve, κ_n the normal curvature of the curve, and τ_r the relative torsion of the curve. $\mathbf{T}$ is the unit tangent, $\mathbf{t}$ the tangent normal and $\mathbf{n}$ the unit normal.

Arbitrary vector fields V and $W \in E^3$ can be expressed as

$$\mathbf{V} = V^i \mathbf{E}_i, \qquad \mathbf{W} = W^i \mathbf{E}_i$$

in the natural basis vectors $\{\mathbf{E}_i, i = 1, 2, 3\}$ of this coordinate system, and we shall note

$$< \mathbf{V}, \mathbf{W} >= V^i W^j \delta_{ij}, \qquad ||\mathbf{V}|| = \sqrt{< \mathbf{V}, \mathbf{V} >}$$

the Euclidean metric and the associated norm for vectors. The Levi-Civita connection on E^3 in Cartesian coordinates is trivial (all Christoffel symbols vanish), and one has

$$\nabla^E_\mathbf{V} \mathbf{W} = (\nabla_\mathbf{V} W^i)\mathbf{E}_i.$$

The Levi-Civita connection on the Riemannian submanifold $\mathcal{M}$, now, is not a trivial one. It is the orthogonal projection of $\nabla^E_\mathbf{V}$ in the tangent bundle $T\mathcal{M}$, so that one has

$$\nabla_\mathbf{V} \mathbf{W} = P_{T\mathcal{M}}[\nabla^E_\mathbf{V} \mathbf{W}] = (\nabla_\mathbf{V} W^i) P_{T\mathcal{M}}[\mathbf{E}_i] \tag{7}$$

where $P_{T\mathcal{M}} : E^3 \mapsto T\mathcal{M}$ is the orthogonal projection operator on $T\mathcal{M}$.

An arbitrary orthonormal local basis $(\mathbf{u}_\mathbf{X}, \mathbf{v}_\mathbf{X}, \mathbf{n})$ for every $\mathbf{X} \in \mathcal{M}$, can be represented through the Euler angles (ψ, γ, ϕ) which are $\mathcal{C}^1$ on $\mathcal{M}$, and with the shorthands $s_\phi \equiv \sin\phi$ and $c_\phi \equiv \cos\phi$, as:

$$\begin{aligned} \mathbf{u}_\mathbf{X} &= \begin{pmatrix} -s_\phi s_\psi c_\gamma + c_\phi c_\psi \\ s_\phi c_\psi c_\gamma + s_\psi c_\phi \\ s_\phi s_\gamma \end{pmatrix}, \\ \mathbf{v}_\mathbf{X} &= \begin{pmatrix} -s_\phi c_\psi - s_\psi c_\phi c_\gamma \\ -s_\phi s_\psi + c_\phi c_\psi c_\gamma \\ s_\gamma c_\phi \end{pmatrix}, \\ \mathbf{n} &= \begin{pmatrix} s_\psi s_\gamma \\ -s_\gamma c_\psi \\ c_\gamma \end{pmatrix} \end{aligned} \tag{8}$$

in the vector basis of E^3.

2.2 Conformal mapping

We are looking for a conformal mapping

$$\begin{array}{rccc} \mathcal{F} & : & \mathcal{P} & \rightarrow & \mathcal{M} \subset E^3 \\ & & \mathbf{P} = (\xi, \eta) & \mapsto & \mathbf{X} = (x^1, x^2, x^3) \end{array} \tag{9}$$

where $\mathcal{P}$ is a parametric space. As finding $\mathcal{F}$ right away is a difficult problem, one focuses instead on finding the 3×2 Jacobian matrix of $\mathcal{F}$

$$J(\mathbf{P}) = (\partial_\xi \mathcal{F}(\mathbf{P}), \partial_\eta \mathcal{F}(\mathbf{P})) \equiv (\tilde{\mathbf{u}}(\mathbf{P}), \tilde{\mathbf{v}}(\mathbf{P})), \tag{10}$$

where $\tilde{\mathbf{u}}, \tilde{\mathbf{v}} \in T\mathcal{M}$ are the columns vectors of J. The mapping $\mathcal{F}$ being conformal, the columns of $J(\mathbf{P})$ have the same norm $L(\mathbf{P}) \equiv ||\tilde{\mathbf{u}}(\mathbf{P})|| = ||\tilde{\mathbf{v}}(\mathbf{P})||$ and are orthogonal to each other, $\tilde{\mathbf{u}}(\mathbf{P}) \cdot \tilde{\mathbf{v}}(\mathbf{P}) = 0$. We can also write:

$$J = L(\mathbf{u}, \mathbf{v}), \qquad \mathbf{n} = \mathbf{u} \wedge \mathbf{v}$$

where

$$\begin{array}{rcl} \mathbf{u} & = & \frac{\tilde{\mathbf{u}}}{||\tilde{\mathbf{u}}||} \\ \mathbf{v} & = & \frac{\tilde{\mathbf{v}}}{||\tilde{\mathbf{v}}||}. \end{array} \tag{11}$$

Recalling that finding a conformal transformation $\mathcal{F}$ is challenging, we will from now on be looking for the Jacobian J, *i.e.*, the triplet $(\mathbf{u}, \mathbf{v}, L)$.

The triplet $(\mathbf{u}, \mathbf{v}, \mathbf{n})$ forms a set of 3 orthonormal basis vectors and can be seen as a rotation of $(\mathbf{u_X}, \mathbf{v_X}, \mathbf{n})$ among the direction $\mathbf{n}$. Therefore, a 2D cross $c(\mathbf{X})$, $\mathbf{X} \in \mathcal{M}$ can be defined with the help of a scalar field θ, where $\mathbf{u} = \mathcal{R}_{\theta,\mathbf{n}}(\mathbf{u_X})$ and $\mathbf{v} = \mathcal{R}_{\theta,\mathbf{n}}(\mathbf{v_X})$, and the local manifold basis $(\mathbf{u_X}, \mathbf{v_X}, \mathbf{n})$ as:

$$\mathbf{u} = c_\theta \mathbf{u_X} + s_\theta \mathbf{v_X}, \qquad \mathbf{v} = -s_\theta \mathbf{u_X} + c_\theta \mathbf{v_X}. \tag{12}$$

By using the Euler angles (ψ, γ, ϕ) and θ, the triplet $(\mathbf{u}, \mathbf{v}, \mathbf{n})$ can also be expressed as:

$$\begin{array}{rcl} \mathbf{u} & = & \begin{pmatrix} -s_{\theta+\phi} s_\psi c_\gamma + c_{\theta+\phi} c_\psi \\ s_{\theta+\phi} c_\psi c_\gamma + s_\psi c_{\theta+\phi} \\ s_{\theta+\phi} s_\gamma \end{pmatrix}, \\ \mathbf{v} & = & \begin{pmatrix} -s_{\theta+\phi} c_\psi - s_\psi c_{\theta+\phi} c_\gamma \\ -s_{\theta+\phi} s_\psi + c_{\theta+\phi} c_\psi c_\gamma \\ s_\gamma c_{\theta+\phi} \end{pmatrix}, \\ \mathbf{n} & = & \begin{pmatrix} s_\psi s_\gamma \\ -s_\gamma c_\psi \\ c_\gamma \end{pmatrix}. \end{array} \tag{13}$$

It is important to note that $\mathbf{u}$ and $\mathbf{v}$ are the two branches of the cross-field $\mathcal{C}_\mathcal{M}$ we are looking for. The projection operator $P_{T\mathcal{M}}$ introduced in Eq. (7) then simply amounts to disregarding the component along $\mathbf{n}$ of vectors.

For a vector field $\mathbf{w}$ defined on $\mathcal{M}$, one can write by derivation of Eq. (13)

$$\begin{aligned} \nabla^E_\mathbf{w} \mathbf{u} &= \mathbf{v}\, \nabla_\mathbf{w}(\theta + \phi) + s_{\theta+\phi} \mathbf{n}\, \nabla_\mathbf{w} \gamma \\ &\quad + (c_\gamma \mathbf{v} - s_\gamma c_{\theta+\phi} \mathbf{n}) \nabla_\mathbf{w} \psi \\ \nabla^E_\mathbf{w} \mathbf{v} &= -\mathbf{u}\, \nabla_\mathbf{w}(\theta + \phi) + c_{\theta+\phi} \mathbf{n}\, \nabla_\mathbf{w} \gamma \\ &\quad + (-c_\gamma \mathbf{u} + s_\gamma s_{\theta+\phi} \mathbf{n}) \nabla_\mathbf{w} \psi \\ \nabla^E_\mathbf{w} \mathbf{n} &= -(s_{\theta+\phi} \mathbf{u} + c_{\theta+\phi} \mathbf{v}) \nabla_\mathbf{w} \gamma \\ &\quad + s_\gamma (c_{\theta+\phi} \mathbf{u} - s_{\theta+\phi} \mathbf{v}) \nabla_\mathbf{w} \psi \end{aligned} \tag{14}$$

and hence, using Eq. (7), the expression of the covariant derivatives on the submanifold $\mathcal{M}$ is:

$$\begin{aligned} \nabla_\mathbf{w} \mathbf{u} &= \mathbf{v}\, \nabla_\mathbf{w}(\theta + \phi) + c_\gamma \mathbf{v} \nabla_\mathbf{w} \psi \\ \nabla_\mathbf{w} \mathbf{v} &= -\mathbf{u}\, \nabla_\mathbf{w}(\theta + \phi) - c_\gamma \mathbf{u} \nabla_\mathbf{w} \psi. \end{aligned} \tag{15}$$

This allows writing the Lie bracket

$$\begin{aligned} [\mathbf{u}, \mathbf{v}] &= \nabla_\mathbf{u} \mathbf{v} - \nabla_\mathbf{v} \mathbf{u} \\ &= -(\mathbf{u} \nabla_\mathbf{u}(\theta + \phi) + \mathbf{v} \nabla_\mathbf{v}(\theta + \phi) \\ &\quad - c_\gamma (\mathbf{u} \nabla_\mathbf{u} \psi + \mathbf{v} \nabla_\mathbf{v} \psi), \end{aligned} \tag{16}$$

which will be used in the upcoming section.

3. INTEGRABILITY CONDITION WITH ISOTROPIC SCALING

The mapping $\mathcal{F}$, now, defines a conformal parametrization of $\mathcal{M}$ if the columns of J commute as vector fields, *i.e.*, if the differential condition

$$0 = [\tilde{\mathbf{u}}, \tilde{\mathbf{v}}] = \nabla_{\tilde{\mathbf{u}}} \tilde{\mathbf{v}} - \nabla_{\tilde{\mathbf{v}}} \tilde{\mathbf{u}} = [L\mathbf{u}, L\mathbf{v}] \tag{17}$$

is verified. Developing the latter expression and posing for convenience $L = e^H$, it becomes

$$0 = \mathbf{v} \nabla_\mathbf{u} H - \mathbf{u} \nabla_\mathbf{v} H + [\mathbf{u}, \mathbf{v}],$$

and then

$$\left\{ \begin{array}{rcl} \nabla_\mathbf{u} H & = & - < \mathbf{v}, [\mathbf{u}, \mathbf{v}] > \\ \nabla_\mathbf{v} H & = & < \mathbf{u}, [\mathbf{u}, \mathbf{v}] > \end{array} \right. \tag{18}$$

which after the substitution of Eq. (16) gives

$$\left\{ \begin{array}{rcl} \nabla_\mathbf{u} H & = & \nabla_\mathbf{v} \theta + \nabla_\mathbf{v} \phi + c_\gamma \nabla_\mathbf{v} \psi \\ -\nabla_\mathbf{v} H & = & \nabla_\mathbf{u} \theta + \nabla_\mathbf{u} \phi + c_\gamma \nabla_\mathbf{u} \psi. \end{array} \right. \tag{19}$$

In order to obtain the boundary value problem for H, the partial differential equation (PDE) governing it will be expressed on $\partial\mathcal{M}$ as well as on the interior of $\mathcal{M}$.

3.1 H PDE on the boundary

As the boundary $\partial\mathcal{M}$ is represented by curves on $\mathcal{M}$, it is possible to parametrize them by arc length and thus associate for each $\mathbf{X} \in \partial\mathcal{M}$ a Darboux frame

$(\mathbf{T}(\mathbf{X}), \mathbf{t}(\mathbf{X}), \mathbf{n}(\mathbf{X}))$. As we are looking for a cross-field $\mathcal{C}_\mathcal{M}$ fulfilling conditions (2), the triplet $(\mathbf{u}, \mathbf{v}, \mathbf{n})$ can be identified as $(\mathbf{T}(\mathbf{X}), \mathbf{t}(\mathbf{X}), \mathbf{n}(\mathbf{X}))$. One then has:

$$\begin{aligned}\partial_s T &= \kappa_g \mathbf{t} + \kappa_n \mathbf{n} \equiv \nabla_\mathbf{u} \mathbf{u} \\ &= \mathbf{v} \nabla_\mathbf{u} \phi + s_\phi \mathbf{n} \nabla_\mathbf{u} \gamma + (c_\gamma \mathbf{v} - s_\gamma c_\phi \mathbf{n}) \nabla_\mathbf{u} \psi\end{aligned}$$

where from follows

$$\left\{ \begin{array}{rcl} \kappa_g &=& \nabla_\mathbf{u} \phi + c_\gamma \nabla_\mathbf{u} \psi \\ \kappa_n &=& s_\phi \nabla_\mathbf{u} \gamma - s_\gamma c_\phi \nabla_\mathbf{u} \psi. \end{array} \right. \tag{20}$$

Using Eq. (19) it becomes:

$$\nabla_\mathbf{t} H = -\kappa_g, \tag{21}$$

the result that matches exactly the one found in the planar case [20].

3.2 H PDE in the smooth region on the interior of M

To find the *PDE* governing H, let's assume the Jacobian J is smooth (and therefore H) in a vicinity $\mathcal{V}$ of $\mathbf{X} \in M$.

We choose $\mathcal{U} \subset \mathcal{V}$ such as $\mathbf{X} \in \mathcal{U}$, $\partial\mathcal{U}$ such as unit tangent vector $\mathbf{T}_0$ to $\partial\mathcal{U}_0$ verifies $\mathbf{T}_0 = \mathbf{v}$, $\mathbf{T}_1$ to $\partial\mathcal{U}_1$ verifies $\mathbf{T}_1 = \mathbf{u}$, $\mathbf{T}_2$ to $\partial\mathcal{U}_2$ verifies $\mathbf{T}_2 = -\mathbf{v}$, $\mathbf{T}_3$ to $\partial\mathcal{U}_3$ verifies $\mathbf{T}_3 = -\mathbf{u}$.

Thus we have a submanifold $\mathcal{U} \subset M$ on which H is smooth, and such as $\partial\mathcal{U} = \partial\mathcal{U}_0 \cup \partial\mathcal{U}_1 \cup \partial\mathcal{U}_2 \cup \partial\mathcal{U}_3$. Darboux frames of $\partial\mathcal{U}$ (Fig. 2) are:

$$\left\{ \begin{array}{rcll} (\mathbf{T}, \mathbf{t}, \mathbf{n}) &=& (\ \mathbf{v}, -\mathbf{u}, \mathbf{n}) & \text{on } \partial\mathcal{U}_0 \\ (\mathbf{T}, \mathbf{t}, \mathbf{n}) &=& (-\mathbf{u}, -\mathbf{v}, \mathbf{n}) & \text{on } \partial\mathcal{U}_1 \\ (\mathbf{T}, \mathbf{t}, \mathbf{n}) &=& (-\mathbf{v}, \ \mathbf{u}, \mathbf{n}) & \text{on } \partial\mathcal{U}_2 \\ (\mathbf{T}, \mathbf{t}, \mathbf{n}) &=& (\ \mathbf{u}, \ \mathbf{v}, \mathbf{n}) & \text{on } \partial\mathcal{U}_3 \end{array} \right. \tag{22}$$

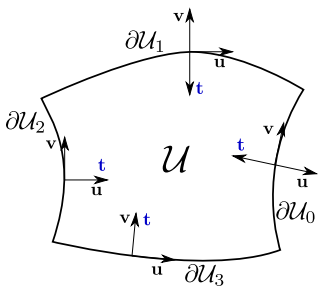

Figure 2: Vicinity of $\mathbf{X}$ considered.

For $(\tilde{\mathbf{u}}, \tilde{\mathbf{v}})$ to be a local coordinate system, we recall Eq. (21) demonstrated in Section 3.1:

$$\kappa_g = -\nabla_\mathbf{t} H, \text{ with } \mathbf{t} = \mathbf{n} \wedge \mathbf{T} \tag{23}$$

and the divergence theorem stating that:

$$\int_{\partial\mathcal{U}} \nabla_\mathbf{t} H = -\int_\mathcal{U} \Delta H. \tag{24}$$

Applying the Gauss-Bonnet theorem on $\mathcal{U}$ leads to:

$$\int_\mathcal{U} K \, \mathrm{d}\mathcal{U} + \int_{\partial\mathcal{U}} \kappa_g \, \mathrm{d}l + 4\frac{\pi}{2} = 2\pi\chi(\mathcal{U})$$

where K and $\chi(\mathcal{U})$ are respectively the Gaussian curvature and the Euler characteristic of $\mathcal{U}$. As $\chi(\mathcal{U}) = 1$ and using Eq. (23) and (24), it becomes:

$$\int_\mathcal{U} K \, \mathrm{d}\mathcal{U} = -\int_\mathcal{U} \Delta H \, \mathrm{d}\mathcal{U} \tag{25}$$

which holds for any chosen $\mathcal{U}$. Hence, there is:

$$\Delta H = -K, \text{ if } J \text{ is smooth.} \tag{26}$$

In the general case, it is impossible for J to be smooth everywhere. Indeed, let's assume $\mathcal{M}$ to be with smooth boundary $\partial\mathcal{M}$ (*i.e.* with no corners) and of the Euler characteristic $\chi(\mathcal{M}) = 1$. If we assume J is smooth everywhere, it becomes:

$$\left\{ \begin{array}{rcl} \int_\mathcal{M} K \, \mathrm{d}\mathcal{M} + \int_{\partial\mathcal{M}} \kappa_g \, \mathrm{d}l &=& 0 \\ 2\pi\chi(\mathcal{M}) &=& 2\pi \end{array} \right. \tag{27}$$

which is not in accordance with the Gauss-Bonnet theorem. Therefore, J has to be singular somewhere in $\mathcal{M}$.

The goal is to build a usable parametrization of $\mathcal{M}$, *i.e.*, being able to use this parametrization to build a quad mesh of $\mathcal{M}$. Therefore, we will allow J to be singular on a finite number N of points $\mathbf{S}_j$, $j \in [|0, N-1|]$ and show that this condition is sufficient for this problem to always have a unique solution.

3.3 H PDE at singular points

For now, we know boundary conditions for H, Eq. (21), and the local equation in smooth regions, Eq. (26). The only thing left is to determine a local PDE governing H at singular points $\{\mathbf{S}_j\}$. We define k_j as the index of singularity $\mathbf{S}_j$.

For this, we are making two reasonable assumptions:

$$\left\{ \begin{array}{rcl} \Delta H(\mathbf{S}_j) &=& -K(\mathbf{S}_j) + \alpha_j \delta(\mathbf{S}_j) \\ k_i &=& k_j \Rightarrow \alpha_i = \alpha_j, \end{array} \right. \tag{28}$$

where α_j is a constant, and δ is the Dirac distribution. We consider the disk $\mathcal{M}$ represented in Fig. 18 with 4 singularities $\mathbf{S}_j, j \in [|0, 3|]$ of index $k_j = 1$.

The Gauss-Bonnet theorem states that:

$$\int_\mathcal{M} K \, \mathrm{d}\mathcal{M} + \int_{\partial\mathcal{M}} \kappa_g \mathrm{d}l = 2\pi\chi(\mathcal{M}).$$

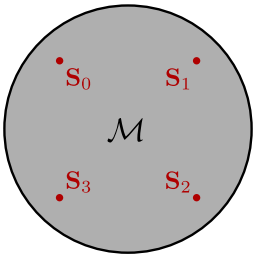

Figure 3: The disk with four singularities of index 1.

Replacing K and κ_g by their values in Eq. (21) and (26), and using the hypothesis (28) we get $\alpha = 2\pi\frac{1}{4}$.

For the singularity of index 1 we have:

$$\Delta H(\mathbf{S}_j) = -K(\mathbf{S}_j) + 2\pi\frac{1}{4}\delta(\mathbf{S}_j).$$

Using the same idea, we can generalize the following:

$$\Delta H(\mathbf{S}_j) = -K(\mathbf{S}_j) + 2\pi\frac{k_j}{4}\delta(\mathbf{S}_j). \tag{29}$$

3.4 Boundary value problem for H

To sum up, the equations governing H on $\mathcal{M}$ are:

$$\left\{\begin{array}{lcll} \Delta H & = & -K + 2\pi\frac{k_j}{4}\delta(\mathbf{S}_j) & \text{on } \mathcal{M} \\ \nabla_{\mathbf{t}} H & = & -\kappa_g & \text{on } \partial\mathcal{M}. \end{array}\right. \tag{30}$$

Eq. (30) being a Laplace equation, with Neumann boundary conditions respecting divergence theorem, it admits a unique solution up to an arbitrary additive constant. A triangulation $\mathcal{M}_T$ of the manifold $\mathcal{M}$ is generated and problem (30) is solved using a finite element formulation with order 1 Lagrange elements. Once H is determined (illustrated in Fig. 4), the next step is to retrieve J's orientation, detailed in the next section. The fact that H is only known up to an additive constant is not harmful as only ∇H will be needed to retrieve J orientation.

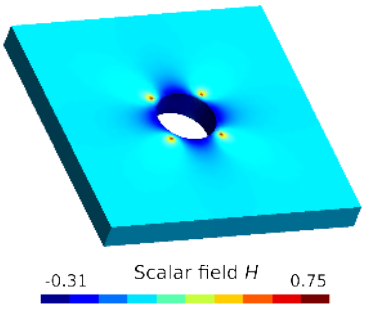

Figure 4: H function obtained on a closed manifold.

3.5 Retrieving crosses orientation from H

In order to get an orientation at a given point $\mathbf{X} \in \mathcal{M}$, a local reference basis $(\mathbf{u_X}, \mathbf{v_X}, \mathbf{n})$ in $\mathbf{X}$ is recalled.

Equation (19) imposes that:

$$\left\{\begin{array}{lcl} \nabla_{\mathbf{u}} H & = & \nabla_{\mathbf{v}}(\phi+\theta) + c_\gamma \nabla_{\mathbf{v}}\psi \\ \nabla_{\mathbf{v}} H & = & -\nabla_{\mathbf{u}}(\phi+\theta) - c_\gamma \nabla_{\mathbf{u}}\psi \end{array}\right. \tag{31}$$

which is equivalent to:

$$\left\{\begin{array}{lcl} \nabla_{\mathbf{u_X}} H & = & \nabla_{\mathbf{v_X}}(\phi+\theta) + c_\gamma \nabla_{\mathbf{v_X}}\psi \\ \nabla_{\mathbf{v_X}} H & = & -\nabla_{\mathbf{u_X}}(\phi+\theta) - c_\gamma \nabla_{\mathbf{u_X}}\psi \end{array}\right. \tag{32}$$

and eventually gives:

$$\left\{\begin{array}{lcl} \nabla_{\mathbf{u_X}}\theta & = & -\nabla_{\mathbf{v_X}} H - \nabla_{\mathbf{u_X}}\phi - c_\gamma \nabla_{\mathbf{u_X}}\psi = P \\ \nabla_{\mathbf{v_X}}\theta & = & \nabla_{\mathbf{u_X}} H - \nabla_{\mathbf{v_X}}\phi - c_\gamma \nabla_{\mathbf{v_X}}\psi = Q \end{array}\right. \tag{33}$$

which is linear in θ.

Using the Kelvin-Stokes theorem, it is possible to show that θ exists if and only if we have:

$$\nabla_{\mathbf{u_X}} Q - \nabla_{\mathbf{v_X}} P = 0. \tag{34}$$

Using Eq. (33) we obtain:

$$\begin{array}{lcl} & & \nabla_{\mathbf{u_X}} Q - \nabla_{\mathbf{v_X}} P \\ & = & \Delta H + \nabla_{\mathbf{v_X}}(c_\gamma \nabla_{\mathbf{u_X}}\psi) - \nabla_{\mathbf{u_X}}(c_\gamma \nabla_{\mathbf{v_X}}\psi) \\ & = & -K + \nabla_{\mathbf{v_X}}(c_\gamma \nabla_{\mathbf{u_X}}\psi) - \nabla_{\mathbf{u_X}}(c_\gamma \nabla_{\mathbf{v_X}}\psi). \end{array} \tag{35}$$

We know that, for 2D manifolds embedded in $\mathbb{R}^3$, the Gaussian curvature K is equal to the Jacobian of the Gauss map of the manifold [27]. We have:

$$\left\{\begin{array}{lcl} \nabla_{\mathbf{u_X}}\mathbf{n} & = & s_\gamma \nabla_{\mathbf{u_X}}\psi \begin{pmatrix} c_\psi \\ s_\psi \\ 0 \end{pmatrix} - \nabla_{\mathbf{u_X}}\gamma \begin{pmatrix} -s_\psi c_\gamma \\ c_\psi c_\gamma \\ s_\gamma \end{pmatrix} \\ \nabla_{\mathbf{v_X}}\mathbf{n} & = & s_\gamma \nabla_{\mathbf{v_X}}\psi \begin{pmatrix} c_\psi \\ s_\psi \\ 0 \end{pmatrix} - \nabla_{\mathbf{v_X}}\gamma \begin{pmatrix} -s_\psi c_\gamma \\ c_\psi c_\gamma \\ s_\gamma \end{pmatrix} \end{array}\right. \tag{36}$$

Therefore we also have:

$$K = s_\gamma(\nabla_{\mathbf{v_X}}\psi \nabla_{\mathbf{u_X}}\gamma - \nabla_{\mathbf{u_X}}\psi \nabla_{\mathbf{v_X}}\gamma). \tag{37}$$

Developing Eq. (35) and substituting K with the right-hand side of Eq. (37) we get:

$$\begin{array}{lcl} & & -K + \nabla_{\mathbf{v_X}}(c_\gamma \nabla_{\mathbf{u_X}}\psi) - \nabla_{\mathbf{u_X}}(c_\gamma \nabla_{\mathbf{v_X}}\psi) \\ & = & -K + c_\gamma \nabla_{\mathbf{v_X}}\nabla_{\mathbf{u_X}}\psi - s_\gamma \nabla_{\mathbf{v_X}}\gamma \nabla_{\mathbf{u_X}}\psi \\ & & -c_\gamma \nabla_{\mathbf{u_X}}\nabla_{\mathbf{v_X}}\psi + s_\gamma \nabla_{\mathbf{u_X}}\gamma \nabla_{\mathbf{v_X}}\psi \\ & = & 0. \end{array} \tag{38}$$

As Eq. (34) is verified, we know that there exists a scalar field θ verifying Eq. (33), and therefore that our problem has a unique solution.

In order to solve Eq. (33), we first need to obtain a smooth global basis $(\mathbf{u_X}, \mathbf{v_X}, \mathbf{n})$ on $\mathcal{M}$. This is possible by generating a branch cut $\mathcal{L}$, as defined below,

and computing a smooth global basis $(\mathbf{u_X}, \mathbf{v_X}, \mathbf{n})$ on $\mathcal{M}$ allowing discontinuities across $\mathcal{L}$.

A branch cut is a set $\mathcal{L}$ of curves of a domain M that do not form any closed loop and that cut the domain in such a way that it is impossible to find any closed loop in $M \backslash \mathcal{L}$ that encloses one or several singularities, or an internal boundary. As we already have a triangulation of M, the branch cut $\mathcal{L}$ is in practice simply a set of edges of the triangulation.

The branch cut is generated with the method described in [20] which is based on [28]. An example of generated branch cut is presented in Fig. 5.

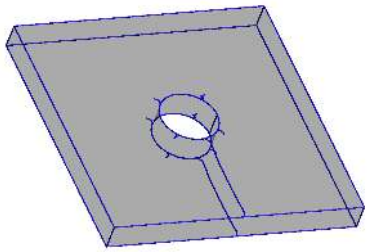

Figure 5: Edges of the branch cut $\mathcal{L}$ are represented in blue. There exists no closed loop in $M \setminus \mathcal{L}$ enclosing one or several singularities.

Once a branch cut $\mathcal{L}$ is available, the field θ can be computed by solving the linear equations (33). With equations (33), θ is known up to an additive constant. For the problem to be well-posed, θ value has to be imposed at one point of domain $\mathcal{M}$. The chosen boundary condition consists in fixing the angle θ at *one* arbitrary point $\mathbf{X}_{BC} \in \partial\mathcal{M}$ so that $\mathcal{C}_{\mathcal{M}}(\mathbf{X}_{BC})$ has one of its branches collinear with $\mathbf{T}(\mathbf{X})$. The problem can be rewritten as the well-posed Eq. (39) and is solved using the finite element method on the triangulation $\mathcal{M}_T$ with order one Crouzeix-Raviart elements. This kind of element has shown to be more efficient for cross-field representation [23].

$$\begin{cases} P_{T\mathcal{M}}(\nabla\theta) & = P_{T\mathcal{M}}(\mathbf{n} \times \nabla H - \nabla\phi - c_\gamma \nabla\psi) \text{ in } \mathcal{M} \\ \theta(\mathbf{X}_{BC}) & = \theta_{\mathbf{X}_{BC}} \text{ for an arbitrary } \mathbf{X}_{BC} \in \partial\mathcal{M} \\ \theta & \text{ discontinuous on } \mathcal{L} \end{cases} \tag{39}$$

It is important to note that for Eq. (39) to be well-posed, the θ value can only be imposed on a *single* point. A consequence is that if $\mathcal{M}$ has more than one boundary ($\partial\mathcal{M} = \partial\mathcal{M}_1 \cup \partial\mathcal{M}_2 \cup \cdots \cup \partial\mathcal{M}_n$), the resulting cross-field is guaranteed to be tangent to the boundary $\partial\mathcal{M}_i$ such as $\mathbf{X}_{BC} \in \partial\mathcal{M}_i$, which does not necessarily hold for all boundaries ∂M_j for $j \neq i$, as detailed in Section 4.1.

Once H and θ scalar fields are computed on $\mathcal{M}$ (illustrated respectively in Fig. 4 and Fig. 6), the cross-field $\mathcal{C}_{\mathcal{M}}$ can be retrieved for all $\mathbf{X} \in \mathcal{M}$:

$$\mathbf{c}(\mathbf{X}) = \{\mathbf{u}_k = \mathcal{R}_{\theta + k\frac{\pi}{2}, \mathbf{n}}(\mathbf{u_X}), k \in [|0, 3|]\}. \tag{40}$$

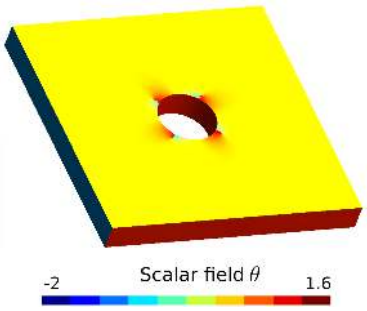

Figure 6: Scalar field θ obtained from scalar field H (represented in Fig. 4).

4. PRELIMINARY RESULTS

As a proof of concept, the cross-field computation based on the imposed singularity configuration is included in the 3-step quad meshing pipeline of [20] (illustrated in Fig. 7 and Fig. 8):

Step 1: impose a singularity configuration, *i.e.*, position and valences of singularities (see [20]).

Step 2: compute a cross-field with the prescribed singularity configuration of Step 1 on an adapted mesh (singularities are placed in refined regions), by solving only two linear systems (Section 3).

Step 3: compute a quad layout on the accurate cross-field of Step 2, and generate a full block-structured isotropic quad mesh (see [23, 20]).

The presented pipeline includes the automatic check that singularity configuration obeys the Euler characteristic of the surface, but it does not inspect all Abel-Jacobi conditions [13, 14, 15]. Further, the models of industrial complexity would require a more robust quad layout generation technique than the one followed here ([23, 20]). The final quad mesh is isotropic, obtained from the quad layout via per-partition bijective parameterization aligned with the smooth cross-field (singularities can only be located on corners of the partitions) [20], and following the size map implied by the H, *i.e.*, the element's edge length is $s = e^H$. In case when the application demands an anisotropic quad mesh, two sizing fields (H_1, H_2) for the cross-field must be computed, more details in Section 5.

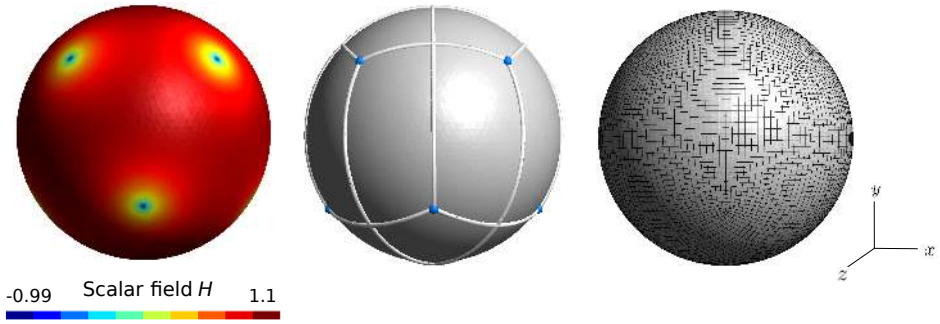

Figure 7: Quad mesh on a 2-sphere with a natural singularity configuration forming an anticube. The singularity configuration comes from solving a non-linear problem, *i.e.*, by using the MBO algorithm from [2].

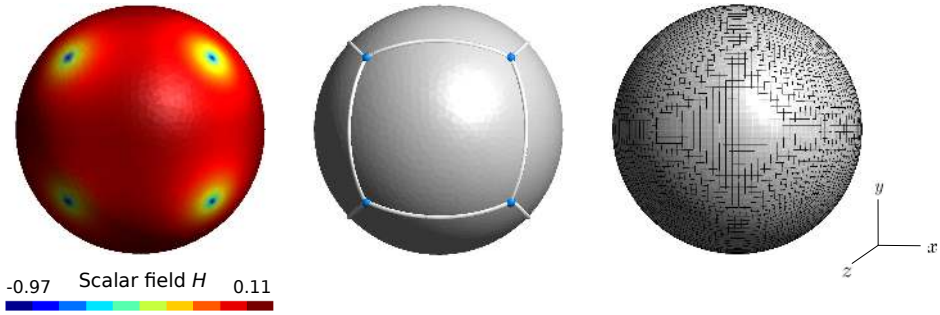

Figure 8: Quad mesh on a 2-sphere with an imposed singularity configuration forming a cube.

4.1 Valid singularity configurations for conformal quad meshing

The singularity configuration, including both the positions and valences, plays a crucial role in the generation of conformal quad meshes [29]. It is essential to note that not all user-imposed singularity configurations matching the Euler's characteristic of the surface will be valid for conformal quad meshing, Fig. 9. The central cause for this lies in the fact that a combination of choices of valences and holonomy is not arbitrary [30]. Relevant findings on the non-existence of certain quadrangulations can be found in [31, 32, 33].

The work of [3] presents the formula for determining the numbers of and indices of singularities, and [34] presents their possible combinations in conforming quad meshes. Latter authors also show that the presented formula is necessary but not sufficient for quad meshes, but neither of these works are proving the rules for the singularities' placement.

Recently, the sufficient and necessary conditions for valid singularity configuration of the conformal quad mesh are presented in the framework based on *Abel-Jacobi's theory* [13, 14, 15]. The developed formulation here is under its direct constraint. In practice, imposing a singularity configuration fulfilling Euler's characteristic constraint ensures that the flat metric, *i.e.*, the H field can be obtained. If this singularity configuration also verifies the holonomy condition, the cross-field will be aligned with all boundaries and consistent across the cut graph.

We recall here that our formulation entitles the user to impose its own singularity configuration, which in practice can contain a suboptimal distribution of singularities. As a consequence, computed cross-field may not be aligned with all boundaries, Fig. 9 d), preventing the generation of the final conformal isotropic quad mesh. To bypass this issue, the following section develops an integrable cross-field formulation with two independent metrics (which are flat except at singularities), instead of only one as presented for Abel-Jacobi conditions.

4.2 Dealing with suboptimal distribution of singularities

The issue of suboptimal distribution of singularities imposes the need for developing a new cross-field formulation on the imposed singularity configuration, which considers the integrability while relaxing the

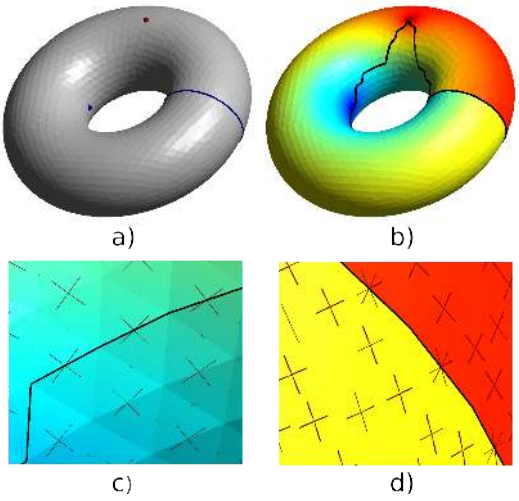

Figure 9: Imposing a $3-5$ singularity configuration on a torus. a) The boundary marked in blue. b) The boundary and the cut graph marked in black. c) Consistent cross-field across the cut graph. d) Cross-field not aligned with the boundary.

condition on isotropic scaling of crosses' branches. More specifically, the integrability condition, along with computing only one scaling field H, $||\tilde{\mathbf{u}}|| = ||\tilde{\mathbf{v}}||$, imposes the strict constraint on the valid singularity configurations, *i.e.*, the need for fulfilling the *Abel-Jacobi theorem*. Therefore, two sizing fields $L_1 = ||\tilde{\mathbf{u}}||$ and $L_2 = ||\tilde{\mathbf{v}}||$ are introduced and the upcoming section presents the mathematical foundations for the generation of an integrable cross-field with anisotropic scaling on $2-$D manifolds. As it will be shown in the following, this setting presents promising results in generating an integrable and boundary-aligned cross-field on the imposed set of singularities, even when their distribution is not fulfilling all Abel-Jacobi conditions. Only for the sake of visual comprehensiveness, the presented motivational examples in Fig. 10 - Fig. 15 are planar.

5. INTEGRABILITY CONDITION WITH ANISOTROPIC SCALING

As explained previously (Section 3), a cross-field $\mathcal{C}_{\mathcal{M}}$ is integrable if and only if $\tilde{\mathbf{u}}$ and $\tilde{\mathbf{v}}$ commute under the Lie Bracket. In other words, the condition:

$$0 = [\tilde{\mathbf{u}}, \tilde{\mathbf{v}}] = \nabla_{\tilde{\mathbf{u}}}\tilde{\mathbf{v}} - \nabla_{\tilde{\mathbf{v}}}\tilde{\mathbf{u}} = [L_1\mathbf{u}, L_2\mathbf{v}] \tag{41}$$

where:

$$L_1 = ||\tilde{\mathbf{u}}||, \qquad L_2 = ||\tilde{\mathbf{v}}|| \tag{42}$$

and

$$\begin{array}{rcl} \mathbf{u} & = & \frac{\tilde{\mathbf{u}}}{||\tilde{\mathbf{u}}||} \\ \mathbf{v} & = & \frac{\tilde{\mathbf{v}}}{||\tilde{\mathbf{v}}||} \end{array} \tag{43}$$

has to be verified.

Developing the latter expression and posing for convenience $L_1 = e^{H_1}$ and $L_2 = e^{H_2}$, it becomes:

$$0 = \mathbf{v}\nabla_{\mathbf{u}}H_2 - \mathbf{u}\nabla_{\mathbf{v}}H_1 + [\mathbf{u}, \mathbf{v}],$$

and then

$$\left\{ \begin{array}{rcl} \nabla_{\mathbf{u}}H_2 & = & - < \mathbf{v}, [\mathbf{u}, \mathbf{v}] > \\ \nabla_{\mathbf{v}}H_1 & = & < \mathbf{u}, [\mathbf{u}, \mathbf{v}] > \end{array} \right. \tag{44}$$

which after the substitution of Eq. (16) gives:

$$\left\{ \begin{array}{rcl} \nabla_{\mathbf{u}}H_2 & = & \nabla_{\mathbf{v}}\theta + \nabla_{\mathbf{v}}\phi + c_\gamma\nabla_{\mathbf{v}}\psi \\ -\nabla_{\mathbf{v}}H_1 & = & \nabla_{\mathbf{u}}\theta + \nabla_{\mathbf{u}}\phi + c_\gamma\nabla_{\mathbf{u}}\psi. \end{array} \right. \tag{45}$$

It is important to note that the three scalar fields (θ, H_1, H_2) are completely defining the cross-field $\mathcal{C}_{\mathcal{M}}$, as (ψ, γ, ϕ) are known since they are defining the local manifold basis $(\mathbf{t}, \mathbf{T}, \mathbf{n})$.

From Eq. (45), we can define the cross-field $\mathcal{C}_{\mathcal{M}}$ integrability error E as:

$$\begin{array}{rl} & E^2(\theta, H_1, H_2) \\ = & \int_{\mathcal{M}} (\nabla_{\mathbf{u}}H_2 - \nabla_{\mathbf{v}}\theta - \nabla_{\mathbf{v}}\phi - c_\gamma\nabla_{\mathbf{v}}\psi)^2 \\ & + (\nabla_{\mathbf{v}}H_1 + \nabla_{\mathbf{u}}\theta + \nabla_{\mathbf{u}}\phi + c_\gamma\nabla_{\mathbf{u}}\psi)^2 \, \mathrm{d}\mathcal{M}. \end{array} \tag{46}$$

The problem of generating an integrable cross-field with anisotropic scaling can therefore be reduced at finding three scalar fields (θ, H_1, H_2) verifying $E(\theta, H_1, H_2) = 0$.

The process of solving this problem presents several difficulties. First, $(\theta, \psi, \gamma, \phi)$ are multivalued functions. This kind of difficulty is commonly encountered in cross-field generation and is tackled here by cutting the domain $\mathcal{M}$ along a generated cut graph. Then, minimizing E regarding (θ, H_1, H_2) is an ill-posed problem. Indeed, there are no constraints on $\nabla_{\mathbf{u}}H_1$ and $\nabla_{\mathbf{v}}H_2$. This is the main obstacle for generating an integrable 2D cross-field with an anisotropic scaling.

A simple approach to solve this problem is proposed here. In order to do so, it is needed to:

- be able to generate a boundary-aligned cross-field matching the imposed singularity configuration,
- compute (H_1, H_2) minimizing E for an imposed $\bar{\theta}$,
- compute θ minimizing E for an imposed $(\bar{H}_1, \bar{H}_2)$.

The final resolution solver (Algorithm 3), proposed in Section 5.4, allows for finding a local minimum for E around an initialization (θ^0, H_1^0, H_2^0).

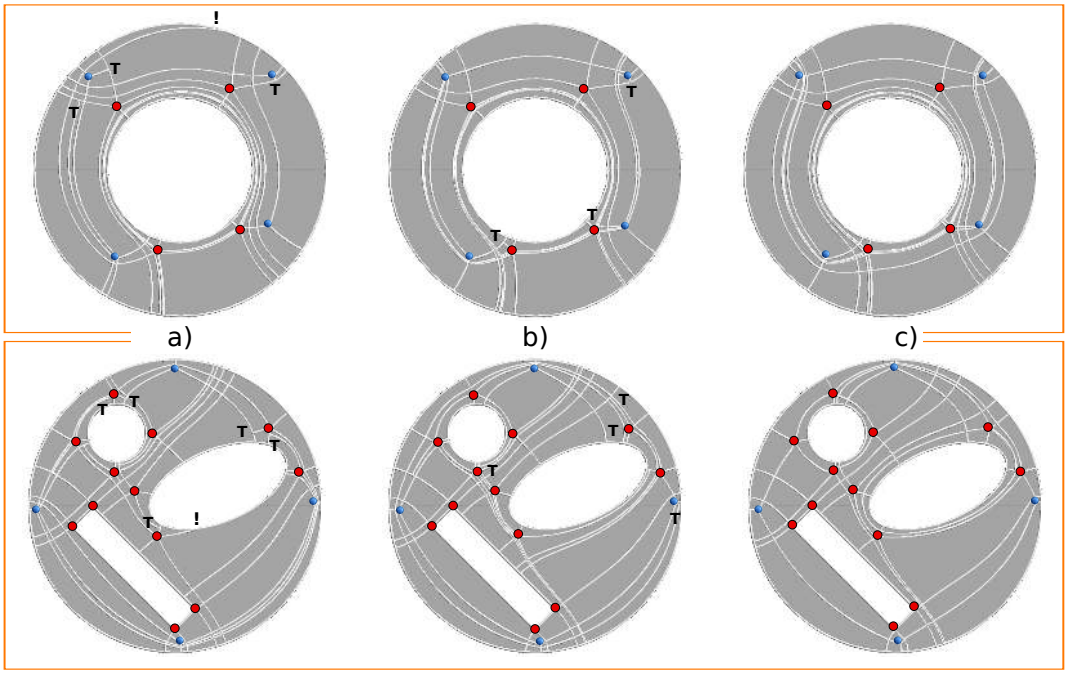

Figure 10: Obtained quad layouts on an imposed set of singularities that do not respect the location's condition from the Abel-Jacobi theorem. a) Quad layouts obtained using the integrable cross-field with isotropic scaling: not aligned with boundaries (marked with "**!**") and demonstrate the presence of t-junctions (marked with "**T**") generated by cutting the limit cycles upon their first orthogonal intersection. b) Quad layouts obtained with imposing the θ value along the cut graph and boundary following the method presented in [28]: boundary aligned but demonstrate the presence of t-junctions (marked with "**T**") generated by cutting the limit cycles upon their first orthogonal intersection. c) Quad layouts obtained using the integrable cross-field with an anisotropic scaling: boundary aligned and without t-junctions.

5.1 Local manifold basis generation and θ initialization

As exposed earlier, in order to completely define a unitary cross-field $\mathcal{C}_\mathcal{M}$ with a scalar field θ it is needed to define a smooth global basis $(\mathbf{t}, \mathbf{T}, \mathbf{n})$ on $\mathcal{M}$. This is possible by generating a branch cut $\mathcal{L}$ and computing a smooth global basis $(\mathbf{t}, \mathbf{T}, \mathbf{n})$ on $\mathcal{M}$ allowing discontinuities across $\mathcal{L}$.

The branch cut is generated using the method described in [28]. A local basis $(\mathbf{t}, \mathbf{T}, \mathbf{n})$ on $\mathcal{M}$ can be generated with any cross-field method. Such local basis will be smooth and will not show any singularities, as discontinuities are allowed across the cut graph $\mathcal{L}$ and no boundary alignment is required. Once the cut graph $\mathcal{L}$ and the local basis $(\mathbf{t}, \mathbf{T}, \mathbf{n})$ are generated, it is possible to compute θ only if:

- θ values on $\partial\mathcal{M}$ are known,
- θ jump values across $\mathcal{L}$ are known.

These can be found using methods described in [28], or can be deduced from a low computational cost cross-field generation detailed in [20].

5.2 Computing (H_1, H_2) from imposed $\bar{\theta}$

For a given $\bar{\theta}$, it is possible to find (H_1, H_2) minimizing E. It is important to note that, in general, there does not exist a couple (H_1, H_2) such as $E = 0$. Minimizing E with imposed $\bar{\theta}$ is finding the couple (H_1, H_2) for which the integrability error is minimal.

The problem to solve is the following:

$$\begin{aligned}&\text{Find } (\bar{H}_1, \bar{H}_2) \text{ such as}\\ &E(\bar{\theta}, \bar{H}_1, \bar{H}_2) = \min_{(H_1,H_2)\in(\mathcal{C}^1(\mathcal{M}))^2} E(\bar{\theta}, H_1, H_2).\end{aligned} \tag{47}$$

Let's define $\mathcal{S}$ as:

$$\mathcal{S} = \{(\bar{H}_1, \bar{H}_2) \mid (\bar{H}_1, \bar{H}_2) \text{ verifies Eq. (47)}\}.$$

For this problem to be well-posed, a necessary condition is to have 2 independent scalar equations involving ∇H_1, and the same for ∇H_2. We can note that in our case, there are no constraints on $\nabla_\mathbf{u} H_1$ and $\nabla_\mathbf{v} H_2$. Therefore, there is only 1 scalar equation involving ∇H_1, and 1 scalar equation involving ∇H_2. As a consequence, the problem we are looking to solve is ill-defined. As this problem is ill-defined, $\mathcal{S}$ will not

be a singleton and, in the general case, there will be more than one solution to the problem (47).

To discuss this problem in detail, we will use the simple example of a planar domain Ω illustrated in Fig. 11.

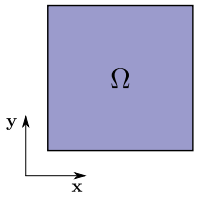

Figure 11: Planar square.

In this case, the unitary frame field $\mathcal{C}_\Omega$ obtained with common methods is:

$$\mathcal{C}_\Omega = \{c(\mathbf{X}) = \{\mathbf{x}, \mathbf{y}, -\mathbf{x}, -\mathbf{y}\}, \mathbf{X} \in \Omega\} \tag{48}$$

which is equivalent to:

$$\bar{\theta} = 0. \tag{49}$$

As in this case domain Ω is planar, we also have:

$$\psi = \gamma = \phi = 0. \tag{50}$$

Equation (45) becomes:

$$\left\{ \begin{array}{rcl} \nabla_{\mathbf{x}} H_2 & = & 0 \\ -\nabla_{\mathbf{y}} H_1 & = & 0 \end{array} \right. \tag{51}$$

which gives:

$$\left\{ \begin{array}{rcl} H_1(x,y) & = & f(x),\ \forall (x,y) \in \Omega,\ \forall f \in \mathcal{C}^1(\mathbb{R}) \\ H_2(x,y) & = & g(y),\ \forall (x,y) \in \Omega,\ \forall g \in \mathcal{C}^1(\mathbb{R}). \end{array} \right. \tag{52}$$

Knowing this, we finally have $\mathcal{S} = (C^1(\mathbb{R}))^2$. There is an infinity of solutions, confirming the fact that problem (47) is ill-defined.

The solution we could expect to obtain for quad meshing purposes would be:

$$\mathcal{S} = \{(H_1, H_2) = (0,0)\}, \tag{53}$$

which is equivalent to $(L_1, L_2) = (1,1)$.

Based on this simple example, we can deduce that problem (47) has to be regularized in order to reduce the solution space. One way to achieve this goal is to add a constraint on the (H_1, H_2) fields we are looking for. A natural one is to look for (H_1, H_2) verifying Eq. (47) and being as smooth as possible.

With this constraint, the problem to solve becomes:

$$\begin{array}{l} \text{Find } (\bar{H}_1, \bar{H}_2) \in \mathcal{S} \text{ such as} \\ \displaystyle\int_{\mathcal{M}} ||\nabla \bar{H}_1||^2 + ||\nabla \bar{H}_2||^2 \, \mathrm{d}\mathcal{M} \\ \displaystyle = \min_{(H_1,H_2)\in\mathcal{S}} \int_{\mathcal{M}} ||\nabla H_1||^2 + ||\nabla H_2||^2 \, \mathrm{d}\mathcal{M}. \end{array} \tag{54}$$

Adding this constraint transforms the linear problem (47) into a non-linear one (54). Algorithm 1 is used to solve Eq. (54), leading to an E's local minimum $(\bar{\theta}, \bar{H}_1, \bar{H}_2)$ close to $(\bar{\theta}, H_1^0, H_2^0)$.

$k = 0$
initial guess H_1^0, H_2^0
compute $\epsilon^0 = E(\bar{\theta}, H_1^0, H_2^0)$
while $\epsilon^k < \epsilon^{k-1}$ **do**
  $k = k + 1$
  find (H_1^k, H_2^k) minimizing:

$$E(\bar{\theta}, f_1, f_2) + \int_{\mathcal{M}} \begin{array}{l} ||\nabla f_1 - \nabla H_1^{k-1}||^2 + \\ ||\nabla f_2 - \nabla H_2^{k-1}||^2 \mathrm{d}\,\mathcal{M}, \end{array}$$

$$(f_1, f_2) \in \left(\mathcal{C}^1(\mathcal{M})\right)^2$$

  compute $\epsilon^k = E(\bar{\theta}, H_1^k, H_2^k)$
end

Algorithm 1: Regularized solver for (H_1, H_2)

5.3 Computing θ from $(\bar{H}_1 \bar{H}_2)$

For an imposed couple $(\bar{H}_1 \bar{H}_2)$, it is possible to find θ minimizing E. The problem to solve is formalized as:

$$\begin{array}{l} \text{Find } \bar{\theta} \in \mathcal{C}^1(\mathcal{M}) \text{ such as} \\ E(\bar{\theta}, \bar{H}_1, \bar{H}_2) = \min\limits_{\theta \in \mathcal{C}^1(\mathcal{M})} E(\theta, \bar{H}_1, \bar{H}_2). \end{array} \tag{55}$$

This problem is non-linear too since $\nabla_{\mathbf{v}} H_1$ and $\nabla_{\mathbf{u}} H_2$ are showing a non-linear dependence regarding θ. Algorithm 2 is used to solve Eq. (55), leading to an E's local minimum $(\bar{\theta}, \bar{H}_1, \bar{H}_2)$ close to $(\theta^0, \bar{H}_1, \bar{H}_2)$.

$k = 0$
initial guess θ^0
deduce $(\mathbf{u}^0, \mathbf{v}^0)$ from θ^0
compute $\epsilon^0 = E(\theta^0, \bar{H}_1, \bar{H}_2)$
while $\epsilon^k < \epsilon^{k-1}$ **do**
  $k = k + 1$
  find θ^k minimizing:

$$\begin{array}{l} E^k(f, \bar{H}_1, \bar{H}_2) \\ \quad = \int_{\mathcal{M}} \begin{array}{l} (\nabla_{\mathbf{u}^{k-1}} \bar{H}_2 - \nabla_{\mathbf{v}^{k-1}} f \\ -\nabla_{\mathbf{v}^{k-1}} \phi - c_\gamma \nabla_{\mathbf{v}^{k-1}} \psi)^2 + \\ (\nabla_{\mathbf{v}^{k-1}} \bar{H}_1 + \nabla_{\mathbf{u}^{k-1}} f \\ +\nabla_{\mathbf{u}^{k-1}} \phi + c_\gamma \nabla_{\mathbf{u}^{k-1}} \psi)^2 \, \mathrm{d}\mathcal{M} \end{array} \end{array}$$

  $f \in \mathcal{C}^1(\mathcal{M})$
  deduce $(\mathbf{u}^k, \mathbf{v}^k)$ from θ^k
  compute $\epsilon^k = E(\theta^k, \bar{H}_1, \bar{H}_2)$;
end

Algorithm 2: Solver for θ

5.4 Minimizing integrability error E regarding (θ, H_1, H_2)

Using the three steps exposed previously, it is possible to find a local minimum in the vicinity of an initialization (θ^0, H_1^0, H_2^0) following Algorithm 3.

$k = 0$
initial guess θ^0 using method presented in Section 5.1
compute (H_1^0, H_2^0) from θ^0 using Alg. 1
compute $\epsilon^0 = E(\theta^0, H_1^0, H_2^0)$
while $\epsilon^k < \epsilon^{k-1}$ **do**
  $k = k + 1$
  compute θ^k from (H_1^{k-1}, H_2^{k-1}) using Alg. 2
  compute (H_1^k, H_2^k) from θ^k using Alg. 1
  compute $\epsilon^k = E(\theta^k, H_1^k, H_2^k)$
end

Algorithm 3: Solver for (θ, H_1, H_2)

For the sake of simplicity the motivational example, presented in Fig. 12 is planar. A set of four of index 1 and four of index -1 singularities whose locations are not fulfilling the Abel-Jacobi condition is imposed. Consequently, a cross-field generated using the H function will not be boundary aligned, and a cross-field generated by imposing the θ value along the cut graph and boundary following the method presented in [28] will not be integrable and therefore will generate limit cycles.

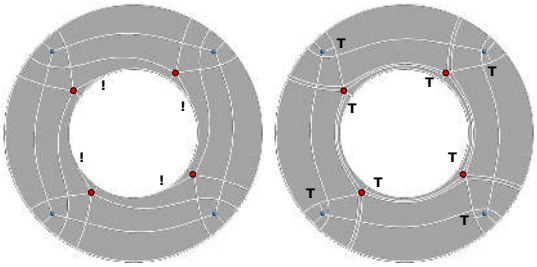

Figure 12: Left: a quad layout obtained using the integrable cross-field with isotropic scaling: not aligned with all boundaries (marked with "**!**"). Right: a quad layout obtained with imposing the θ value along the cut graph and boundary following the method presented in [28]: boundary-aligned but with t-junctions (marked with "**T**") generated by cutting the limit cycles upon their first orthogonal intersection.

The method presented here is applied to compute an integrable boundary-aligned cross-field. Fig. 13 represents the cross-field used as an initial guess and Fig. 14 is the one obtained at Algorithm 3 convergence.

Fig. 13 demonstrates that integrability error density is not concentrated in certain regions, but rather quite uniformly spread over the domain. This suggests that

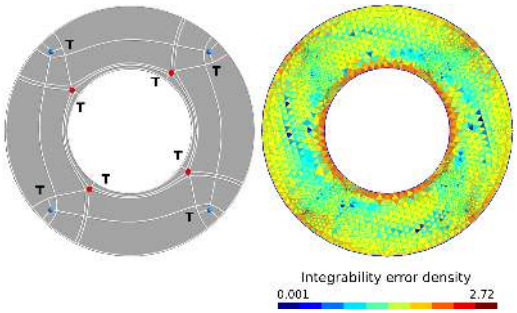

Figure 13: Left: a quad layout obtained at initialization: boundary-aligned but with t-junctions (marked with "**T**"). Right: the integration error density on Ω. The total integration error is $E = 0.307898$.

addressing the integrability issue cannot be performed via local modifications but only via the global one, *i.e.*, the convergence of the presented non-linear problem. Fig. 14 shows that generating a limit cycle-free 2D cross-field can indeed be done by solving Eq. (45). Nevertheless, this problem is highly non-linear and ill-defined, and solving it turns out to be difficult.

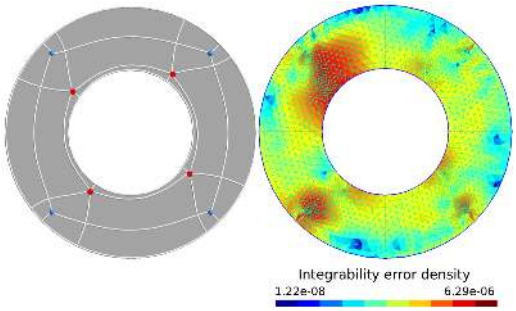

Figure 14: Left: a quad layout obtained from integrable cross-field with an anisotropic scaling: orthogonal with all boundaries and without t-junctions. Right: the integration error density on Ω. The total integration error at convergence is $E = 1.45639e - 06$.

The method proposed here works well when initialization is not far from an integrable solution, *i.e.*, when the imposed singularity set obeys Abel-Jacobi's conditions. Otherwise, it does not converge up to the desired solution by reaching a local minimum $(\bar{\theta}, \bar{H}_1, \bar{H}_2)$ which does not satisfy $E(\bar{\theta}, \bar{H}_1, \bar{H}_2) = 0$, as illustrated in Fig. 15. Although, it is interesting to note that, even without the presented method's convergence, the number of t-junctions dramatically decreases and the valid solution, in the opinion of authors, can be "intuitively presumed".

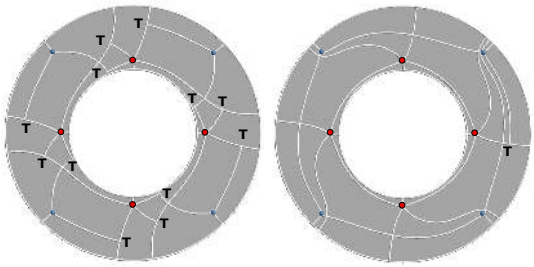

Figure 15: Left: a quad layout obtained at initialization, with t-junctions (marked with "**T**"), the total integration error is $E = 0.842169$. Right: a quad layout obtained at convergence, the total integration error is $E = 0.013597$.

6. CONCLUSION AND FUTURE WORK

We presented the mathematical foundations for the generation of an integrable cross-field on 2D manifolds based on a user-imposed singularity configuration with both isotropic and anisotropic scaling. Here, the mathematical setting is constrained by the Abel-Jacobi conditions for a valid singularity pattern. With the automatic algorithms to check and optimize the singularity configuration (as recently presented in [13, 14, 15]), the developed framework can be used to effectively generate both an isotropic and an anisotropic block-structured quad mesh with prescribed singularity distribution. When it comes to computational costs of our cross-field generation, the formulation with isotropic scaling H takes solving only two linear systems, and the anisotropic one (H_1, H_2) represents a non-linear problem.

An attractive direction for future work includes, although it is not limited to, working with the user-imposed size map. By using the integrable cross-field formulation relying on two sizing fields H_1 and H_2, it would be possible to take into account the anisotropic size field to guide the cross-field generation. The size field obtained from the generated cross-field would not precisely match the one prescribed by the user, but it would be as close as possible to the singularity configuration chosen for the cross-field generation.

It is important to note that employing the presented framework in the 3D volumetric domain would be possible only for a limited number of cases, in which the geometric and topological characteristics of the volume (more details in [34, 35]) allow the use of cross-field guided surface quad mesh for generating a hex mesh.

A. ADDITIONAL EXAMPLES

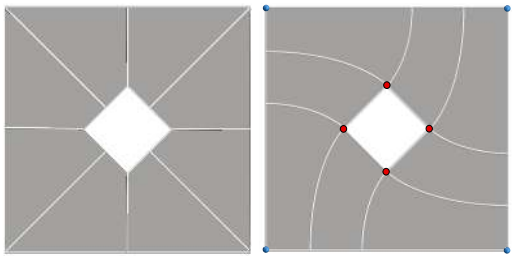

Figure 16: A square with a squared hole rotated by $\frac{\pi}{4}$. Left: Quad layout obtained for an empty singularity set. The corresponding cross-field is isotropic, boundary aligned and integrable. Right: Quad layout obtained for a singularity set composed of four valence 3 (in blue) and four valence 5 (in red) singularities. The corresponding cross-field is anisotropic, boundary aligned and integrable.

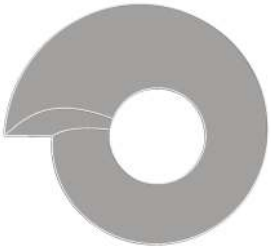

Figure 17: Nautilus with a hole. Quad layout obtained for an empty singularity set. The corresponding cross-field is isotropic, boundary aligned and integrable.

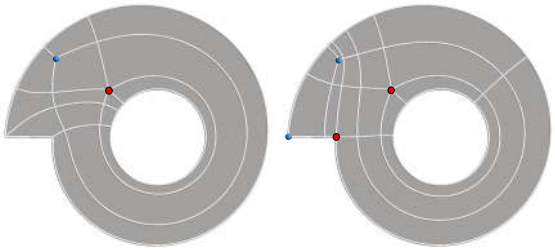

Figure 18: Nautilus with a hole. Left: Quad layout obtained for a singularity set composed of a valence 3 (in blue) and a valence 5 (in red) singularity. The corresponding cross-field is anisotropic, boundary aligned and integrable. Right: Quad layout obtained for a singularity set composed of two valence 3 (in blue) and two valence 5 (in red) singularity. The corresponding cross-field is anisotropic, boundary aligned and integrable.

References

[1] Bommes D., Lévy B., Pietroni N., Puppo E., Silva C.T., Tarini M., Zorin D. "Quad Meshing." *Eurographics (STARs)*, pp. 159–182. 2012

[2] Viertel R., Osting B. "An approach to quad meshing based on harmonic cross-valued maps and the Ginzburg–Landau theory." *SIAM Journal on Scientific Computing*, vol. 41, no. 1, A452–A479, 2019

[3] Beaufort P.A., Lambrechts J., Henrotte F., Geuzaine C., Remacle J.F. "Computing cross fields A PDE approach based on the Ginzburg-Landau theory." *Procedia engineering*, vol. 203, 219–231, 2017

[4] Bunin G. "A continuum theory for unstructured mesh generation in two dimensions." *Computer Aided Geometric Design*, vol. 25, no. 1, 14–40, 2008

[5] Ben-Chen M., Gotsman C., Bunin G. "Conformal flattening by curvature prescription and metric scaling." *Computer Graphics Forum*, vol. 27, pp. 449–458. Wiley Online Library, 2008

[6] Kälberer F., Nieser M., Polthier K. "Quadcover-surface parameterization using branched coverings." *Computer graphics forum*, vol. 26, pp. 375–384. Wiley Online Library, 2007

[7] Ray N., Li W.C., Lévy B., Sheffer A., Alliez P. "Periodic global parameterization." *ACM Transactions on Graphics (TOG)*, vol. 25, no. 4, 1460–1485, 2006

[8] Lyon M., Campen M., Kobbelt L. "Quad layouts via constrained t-mesh quantization." *Computer Graphics Forum*, vol. 40, pp. 305–314. Wiley Online Library, 2021

[9] Lyon M., Campen M., Kobbelt L. "Simpler quad layouts using relaxed singularities." *Computer Graphics Forum*, vol. 40, pp. 169–180. Wiley Online Library, 2021

[10] Campen M., Zorin D. "Similarity maps and field-guided T-splines: a perfect couple." *ACM Transactions on Graphics (TOG)*, vol. 36, no. 4, 1–16, 2017

[11] Ebke H.C., Schmidt P., Campen M., Kobbelt L. "Interactively controlled quad remeshing of high resolution 3d models." *ACM Transactions on Graphics (TOG)*, vol. 35, no. 6, 1–13, 2016

[12] Tong Y., Lombeyda S., Hirani A.N., Desbrun M. "Discrete multiscale vector field decomposition." *ACM transactions on graphics (TOG)*, vol. 22, no. 3, 445–452, 2003

[13] Chen W., Zheng X., Ke J., Lei N., Luo Z., Gu X. "Quadrilateral mesh generation I: Metric based method." *Computer Methods in Applied Mechanics and Engineering*, vol. 356, 652–668, 2019

[14] Lei N., Zheng X., Luo Z., Luo F., Gu X. "Quadrilateral mesh generation II: Meromorphic quartic differentials and Abel–Jacobi condition." *Computer Methods in Applied Mechanics and Engineering*, vol. 366, 112–980, 2020

[15] Zheng X., Zhu Y., Chen W., Lei N., Luo Z., Gu X. "Quadrilateral mesh generation III: Optimizing singularity configuration based on Abel–Jacobi theory." *Computer Methods in Applied Mechanics and Engineering*, vol. 387, 114–146, 2021

[16] Crane K., Desbrun M., Schröder P. "Trivial connections on discrete surfaces." *Computer Graphics Forum*, vol. 29, pp. 1525–1533. Wiley Online Library, 2010

[17] Myles A., Zorin D. "Controlled-distortion constrained global parametrization." *ACM Transactions on Graphics (TOG)*, vol. 32, no. 4, 1–14, 2013

[18] Myles A., Zorin D. "Global parametrization by incremental flattening." *ACM Transactions on Graphics (TOG)*, vol. 31, no. 4, 1–11, 2012

[19] Campen M., Shen H., Zhou J., Zorin D. "Seamless parametrization with arbitrary cones for arbitrary genus." *ACM Transactions on Graphics (TOG)*, vol. 39, no. 1, 1–19, 2019

[20] Jezdimirović J., Chemin A., Reberol M., Henrotte F., Remacle J.F. "Quad layouts with high valence singularities for flexible quad meshing." *Proceedings of the 29th Meshing Roundtable*, 2021

[21] Shepherd K.M., Hiemstra R.R., Hughes T.J. "The Quad Layout Immersion: A Mathematically Equivalent Representation of a Surface Quadrilateral Layout." *arXiv preprint arXiv:2012.09368*, 2020

[22] Bommes D., Campen M., Ebke H.C., Alliez P., Kobbelt L. "Integer-grid maps for reliable quad meshing." *ACM Transactions on Graphics (TOG)*, vol. 32, no. 4, 1–12, 2013

[23] Jezdimirović J., Chemin A., Remacle J.F. "Multiblock decomposition and meshing of 2D domain using Ginzburg-Landau PDE." *Proceedings, 28th International Meshing Roundtable*, 2019

[24] Vaxman A., Campen M., Diamanti O., Panozzo D., Bommes D., Hildebrandt K., Ben-Chen M. "Directional field synthesis, design, and processing." *Computer Graphics Forum*, vol. 35, pp. 545–572. Wiley Online Library, 2016

[25] Hertzmann A., Zorin D. "Illustrating smooth surfaces." *Proceedings of the 27th annual conference on Computer graphics and interactive techniques*, pp. 517–526. 2000

[26] Knöppel F., Crane K., Pinkall U., Schröder P. "Globally optimal direction fields." *ACM Transactions on Graphics (TOG)*, vol. 32, no. 4, 1–10, 2013

[27] Singer I.M., Thorpe J.A. *Lecture notes on elementary topology and geometry*. Springer, 2015

[28] Bommes D., Zimmer H., Kobbelt L. "Mixed-integer quadrangulation." *ACM Transactions On Graphics (TOG)*, vol. 28, no. 3, 1–10, 2009

[29] Gu X., Luo F., Yau S.T. "Computational conformal geometry behind modern technologies." *Notices of the American Mathematical Society*, vol. 67, no. 10, 1509–1525, 2020

[30] Myles A., Pietroni N., Zorin D. "Robust Field-aligned Global Parametrization: Supplement 1, Proofs and Algorithmic Details." *Visual Computing Lab*, 2014

[31] Barnette D., Jucovič E., Trenkler M. "Toroidal maps with prescribed types of vertices and faces." *Mathematika*, vol. 18, no. 1, 82–90, 1971

[32] Jucovič E., Trenkler M. "A theorem on the structure of cell–decompositions of orientable 2–manifolds." *Mathematika*, vol. 20, no. 1, 63–82, 1973

[33] Izmestiev I., Kusner R.B., Rote G., Springborn B., Sullivan J.M. "There is no triangulation of the torus with vertex degrees 5, 6,..., 6, 7 and related results: Geometric proofs for combinatorial theorems." *Geometriae Dedicata*, vol. 166, no. 1, 15–29, 2013

[34] Fogg H.J., Sun L., Makem J.E., Armstrong C.G., Robinson T.T. "Singularities in structured meshes and cross-fields." *Computer-Aided Design*, vol. 105, 11–25, 2018

[35] White D.R., Tautges T.J. "Automatic scheme selection for toolkit hex meshing." *International Journal for Numerical Methods in Engineering*, vol. 49, no. 1-2, 127–144, 2000